

Global Biogeochemical Cycles®

RESEARCH ARTICLE

10.1029/2024GB008136

Dongsheng Liu and Qiuwen Chen
 contributed equally to this work.

Nitrogen Cycling in Reservoir Drawdown Areas and the Impacts on Water Quality

Dongsheng Liu^{1,2,3}, Qiuwen Chen^{1,2,3} , Taylor Maavara⁴ , Jianyun Zhang^{1,2}, and Yuchen Chen^{1,3}

¹The National Key Laboratory of Water Disaster Prevention, Nanjing Hydraulic Research Institute, Nanjing, China,

²Yangtze Institute for Conservation and Development, Nanjing, China, ³Center for Eco-Environment Research, Nanjing Hydraulic Research Institute, Nanjing, China, ⁴School of Geography, University of Leeds, Leeds, UK

Key Points:

- The drawdown area (DA) is a net source of nitrogen (N) to the Three Gorges Reservoir water column within a full hydrological cycle
- About 30% of the total N load to the water column from the reservoir DA is mitigated by the sediment through denitrification and capture
- N release from the reservoir DA mainly occurs during the drying period, whereas N removal from the water column mainly occurs during flooding

Supporting Information:

Supporting Information may be found in the online version of this article.

Correspondence to:

Q. Chen,
qwchen@nhri.cn

Citation:

Liu, D., Chen, Q., Maavara, T., Zhang, J., & Chen, Y. (2024). Nitrogen cycling in reservoir drawdown areas and the impacts on water quality. *Global Biogeochemical Cycles*, 38, e2024GB008136. <https://doi.org/10.1029/2024GB008136>

Received 13 FEB 2024
 Accepted 29 MAY 2024

Abstract Reservoir drawdown areas (DAs) can be both important nitrogen (N) sources to river networks and hot spots for N removal from freshwater ecosystems. The net effect of DAs on the N availability in reservoirs within a full hydrological cycle remains unclear. In this paper, the N dynamics in the DA of the Three Gorges Reservoir, Yangtze River, China, are investigated through a combination of discrete and continuous in situ observations and sampling over a span of 2 years, complemented by numerical modeling. We show that the DA is a net source of N to the water column, and that about 30% of the total annual N load released from the DA is mitigated by the sediment through denitrification and capture. The annual net load of the total N from the DA to the reservoir is ca. 0.59 kg per meter along the river, which is on the same order of magnitude as the input load from the density current of the Yangtze River to its tributaries, generally considered to be the primary driver of eutrophication in tributaries. N release in the DA mainly occurs during the drying period, whereas denitrification in the sediment mostly takes place during the flooding period when the oxido-reducing potential is low. Our findings quantify and therefore clarify the N source/sink dynamics from the DA to the reservoir, offering a new perspective on the importance of DA nutrient loading in decision-making related to integrated management of inundated lands to alleviate reservoir eutrophication by river damming.

Plain Language Summary Nitrogen (N) is an essential nutrient element, but it can be harmful to water quality in excess amounts. Drawdown areas (DAs) are regions at the edges of reservoirs that are alternately flooded and dried as water levels rise and fall. In some conditions, DAs can cause N pollution by adding N to the reservoirs, while in other conditions, DAs can alleviate pollution by removing N from the reservoir by turning it into a gas through the process of denitrification. The annual balance for these pollution-driving versus pollution-alleviating processes across the entire year remains unclear. Based on 2 years of continuous field observations and modeling of N cycling in the DA of the Three Gorges Reservoir, China, this paper finds that annually sediment denitrification and retention in the DA eliminates 30% of the N load released from the sediment itself. N release in the DA mainly occurs when reservoir water level falls as the weather warms up. Denitrification, which turns nitrate into a gas that can leave the reservoir and enter the atmosphere, in sediment under high water levels is the main mechanism that removes N from the DAs. We find that the amount of N released to the reservoir from the DAs is similar in size to the N load received from the upstream river, and thus needs to be considered in reservoir water quality management decisions.

1. Introduction

Dam reservoirs are constructed because they can present socioeconomic benefits, including flood control. Among the 23,853 purpose-specific global reservoirs tabulated in the Global Dam Tracker database (Zhang & Gu, 2023), nearly 10% have the primary function of flood control. This number is tripled when all reservoirs with flood control as one of the functions are considered (Liu, 2022). Reservoir drawdown areas (DA) are subject to manual regulation corresponding to dam operation, driving large fluctuations in water level and a wide area around a reservoir perimeter that is periodically inundated and then dried (Bao et al., 2015). Reservoirs with flood control as the primary function usually have large DAs around their perimeter, accounting for 10%–25% of the surface area of a reservoir at its maximum filling level (Keller et al., 2021). The DAs of flood control reservoirs often reverse the natural timeframe of alternating wetting and drying; that is, wet during the natural dry season, and vice versa (Bao et al., 2015; He et al., 2020).

Watershed managers and local stakeholders often anecdotally assume that the DAs of flood control reservoirs cause nitrogen (N) release and therefore N pollution to the reservoir water column, but scientific evidence remains

unclear. In dry seasons, reservoir impoundment quickly inundates the DA, driving sediment N release to the reservoir via diffusion (S. Wang et al., 2019; Xu et al., 2010). The decomposition of flooded vegetation in the DA can also act as a means for the release of N nutrients to the water column. For example, Chang and Wen (1997) found that the nutrients released from the decay of plants in the DAs were a key driver of the surge in total nitrogen (TN) during the early stage of reservoir impoundment. Similarly, Xiao et al. (2017) showed via in situ experimental decomposition of plants carried out in the Three Gorges Reservoir (TGR) that the TN load from the dominant plant species in the DA reached 81.1 kg ha^{-1} , a flux high enough to damage the aquatic environment of the reservoir by promoting eutrophication, which tends to occur in this system at TN concentrations in excess of 1.3 mg/L (Tang et al., 2016). In several studies of reservoirs in the US and China, the DA was considered a non-negligible contributor to the increased risk of reservoir eutrophication (Chen et al., 2019; Gao et al., 2016; Harrison et al., 2017; Lin et al., 2019).

Conversely, DAs are also known as the “liver” of rivers due to their self-purification function (Brunke & Gonser, 1997; Fischer et al., 2005; Zhao et al., 2020). Sequential wetting and drying cycles enable frequent hyporheic exchange between surface water and sediment pore water in reservoir DAs. Rising water levels during rewetting carry dissolved inorganic nitrogen (DIN), mainly in the forms of ammonium ($\text{NH}_4^+\text{-N}$) and nitrate ($\text{NO}_3^-\text{-N}$), dissolved oxygen (DO), and dissolved organic carbon, into the sediment, promoting nitrification and aerobic respiration (Gu et al., 2012), thus removing harmful $\text{NH}_4^+\text{-N}$ from the water column. With the continuous consumption of DO, denitrification dominates the outflow path during water level decline. This process efficiently converts nitrate N into gaseous N and escapes from the system (Shuai et al., 2017). Moreover, periodic water level fluctuation improves the abundance and diversity of microorganisms (Deng et al., 2023; Ye et al., 2017), enabling nitrification, aerobic respiration, and denitrification and thereby the removal of DIN in DAs. Recent studies have also shown the role of reservoir DAs as hotspots of emissions of N_2 , the end-product of denitrification, and nitrous oxide, a byproduct of nitrification and an intermediate in denitrification (Li et al., 2015; Shi et al., 2021), which indicates that sediment with dry–wet alternation serves as a primary site for N removal (Mulholland et al., 2008; Shi et al., 2020; Trauth et al., 2018). In addition to denitrification, DAs can commonly retain a portion of infiltrated solutes and serve as an N sink (Liu et al., 2019; Mahmood et al., 2019; Welch et al., 2013).

Whether DAs have a net positive or negative effect on the N water quality of reservoirs within a full hydrological cycle, that is, a complete wetting and drying period, remains unclear. The characteristics of N cycling in DAs and the underlying mechanism need to be more fully quantified across seasons. In this paper, the N dynamics, budgets, and associated exchange mechanisms for DIN, organic nitrogen (ON), and TN in the DA of the TGR, China are quantified through in situ monitoring, laboratory experiments, and numerical modeling. The paper primarily aims to (a) reveal the dominant process of N cycling in the DA under different hydrological conditions, (b) clarify the hydrological mechanism associated with the drivers of N cycling, and (c) quantify the annual budget of the net TN load to the water column from the DA.

2. Materials and Methods

2.1. Study Area and Sampling Sites

The TGR on the Yangtze River in China is the largest flood control reservoir in the world (Wang et al., 2021), with a total surface area of $1,084 \text{ km}^2$. The reservoir volume is generally reduced to the flood control minimum limit in wet seasons (June to August), and a high water level is maintained during dry seasons (November to January) with a total water level variation range of $145\text{--}175 \text{ m}$ (Yu et al., 2020). When the DA is exposed, a wide range of hygrophilic herbs grow, but their growth is abruptly halted due to the impoundment of the reservoir at the end of their growing season. The Pengxi River is the largest tributary of the TGR and is representative of most other tributaries in terms of regional geographical, geological, and climatic characteristics (Bao et al., 2015). The DA in the Pengxi River region covers approximately 56.60 km^2 , accounting for 16.27% of the total TGR's DA, the largest of any tributary (Figure S1 in Supporting Information S1) (Jin et al., 2021).

The DA in the middle reaches of the Pengxi River in Gaoyang (GY) was selected for this study (Figure 1). The DA here is free of agricultural activity, and the water bodies around it are minimally affected by potentially confounding N fluxes from the density current in the mainstream of the Yangtze River (Xiang et al., 2021a), thus providing an ideal region for analyzing the effect of DAs on reservoir water quality. The sediment sampling site is located at an elevation of 146.5 m in the DA (GY, $31^\circ 5' 48.2'' \text{ N}$ and $108^\circ 40' 20.1'' \text{ E}$), which becomes mostly

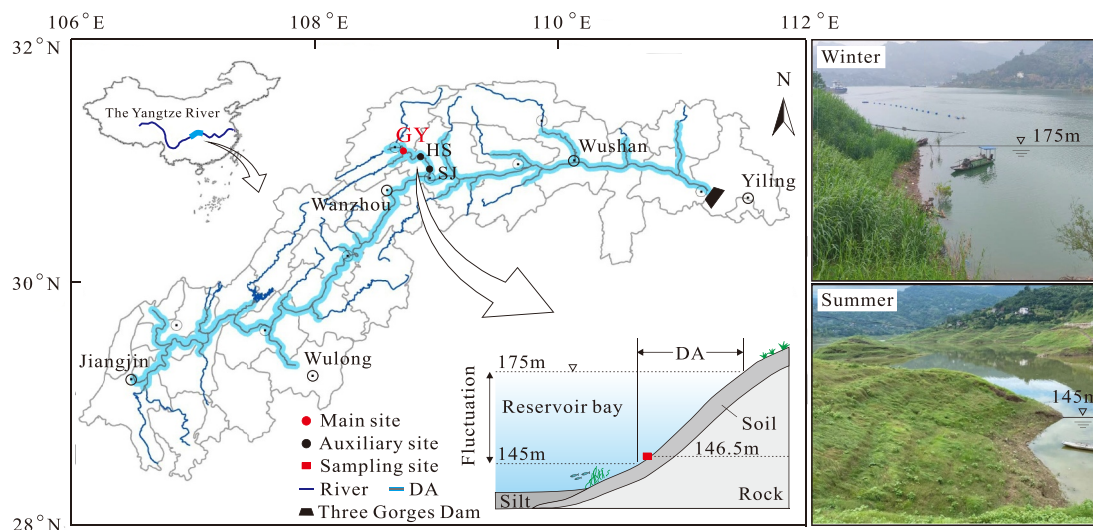


Figure 1. Locations of the study area and sampling sites. The mean sea level is the reference point for elevation. DA, drawdown area; GY, Gaoyang; HS, Huangshi; and SJ, Shuangjiang.

submerged at high water levels. To validate the spatial trends in the N cycling response to the wetting–drying cycles, two auxiliary sites in the DAs of the Pengxi River region (Figure 1), Huangshi (HS, 30°59′47.5″ N and 108°42′55.0″ E) and Shuangjiang (SJ, 30°56′54.1″ N and 108°39′56.0″ E), were selected for comparative study.

2.2. In Situ Monitoring

Precipitation in the Pengxi River region was recorded at 15-min intervals using a portable weather station (RG3-M; Onset HOBO, MA, USA), as shown in Figure S2a in Supporting Information S1. At the GY site, the water pressure, temperature, oxido-reducing potential (ORP), and DO were measured at 1 hr intervals through the online monitoring and remote transmission system installed in the DA's sediment–water interface (Figure S2b in Supporting Information S1), whereas at the HS and SJ sites, these parameters were recorded at 1 hr frequency by employing Onset HOBO data loggers (U20–001 and U26–001, respectively; MA, USA). Chlorophyll-a in the water profiles (≥ 146.5 m) at all sites was measured at monthly frequency using a multiparameter water quality meter (YSI; Yellow Springs, OH, USA) (Figure S2 in Supporting Information S1). All equipment and instruments were calibrated, cleaned, and maintained as needed, and at minimum according to recommended manufacturer frequencies.

2.3. Sample Collection, Pretreatment, and Analysis

A rectangular area of approximately 3 m² around each sediment sampling site (Figure 1) was selected for the collection of sediments and water. At the GY site, the sampling time ran through two full hydrological years (from June 2018 to May 2020), and the samples were collected at two time points in each of the four periods (low-water-level period [LWP], flooding period [FP], high-water-level period [HWP], and drying period [DP]) (Figure S3 in Supporting Information S1), yielding 16 sampling times. For the comparative study, sampling was conducted at all three sites during a representative flooding–drying cycle in the LWP (June 7–30, 2016), and the samples were collected 16 times throughout the process at each site. The water level of the representative flooding–drying cycle, determined via the Froude similarity criterion (Christensen & Frigaard, 1994), namely, time scale = geometric scale^{1/2}, based on the prototype of annual water level change from 145 to 175 m, was considered practicable for research on the spatial trends in the N cycling response to annual wetting–drying cycle in the DA (Text S1 in Supporting Information S1).

At each sampling time, a total of 12 L of overlying water (the water adjacent to the sediment–water interface) was collected preferentially using a polymethyl methacrylate (PMMA) water collector (4 L). The 1.5 L water sample was immediately filtered (0.45 μ m) for cryopreservation and analysis, and the rest was used for culture

experiments. Six sediment cores were collected at each time point using a Rigo Co. gravity corer ($\phi 90$ mm \times 600 mm). The upper 20 cm of the sediment cores was transferred into tailored plexiglass tubes ($\phi 90$ mm \times 350 mm) and covered by approximately 10 cm high in situ water. Three replicates were stored for 24 hr pending use in flow culture experiments (Section 2.4.1), whereas the three other replicates were directly used for release tests (Section 2.5.1). Finally, surface sediments (3 cm thick) were collected using an Ekman grab sampler in triplicate and homogenized. A total of 200 g of the homogenized samples was saved in 50 mL tubes and frozen for N component analysis; 20 g samples were stored in Eppendorf tubes, sealed, and kept at -80°C until scheduled microbial analysis; the rest was evenly placed in 12 PVC pipes ($\phi 40$ mm \times 150 mm) and served as samples for static culture experiments (Section 2.4.2).

Sample analysis in water and sediment was based on standard methods (Ministry of Environmental Protection of China, 2002) (Table S1 in Supporting Information S1). The concentrations of $\text{NH}_4^+\text{-N}$, $\text{NO}_3^-\text{-N}$, $\text{NO}_2^-\text{-N}$, total dissolved nitrogen (TDN), and TN in water were determined spectrophotometrically (DR6000, HACH Co., USA). Total suspended solids (TSS) were measured via the filter membrane weighing method (0.45 μm). Sediments were freeze-dried (ALPHA 2–4 LSC, Martin Christ Co. Ltd., Germany) and ground prior to analysis. Sediment TN was determined using the Kjeldahl digestion method with $\text{K}_2\text{Cr}_2\text{O}_7\text{-H}_2\text{SO}_4$. Sediment IN (pore-water DIN + particulate IN) was extracted via oscillation with 2 mol L^{-1} of KCl, and the supernatant was extracted using a 5 mL pipette and then filtered through a 0.45 μm membrane. The supernatant concentrations of $\text{NH}_4^+\text{-N}$, $\text{NO}_3^-\text{-N}$, and $\text{NO}_2^-\text{-N}$ were determined using Nessler's reagent colorimetry, UV spectrophotometry, and diazo coupling spectrophotometry, respectively. Standard curves were generated for the analysis of N species in all samples with a quality threshold of $r^2 = 0.99$ for $p < 0.01$. The abundances of mineralizing, nitrifying, denitrifying, and anammox microorganisms in the sediment were determined through quantitative polymerase chain reaction by using *Urec*, *AOB*, *nirS*, and *hzsB* as marker genes, respectively (Table S2 in Supporting Information S1), and the sample recovery efficiencies were 100.84%, 85.20%, 97.68%, and 86.76%, respectively. Microbial analysis was conducted by Shanghai Meiji Biomedical Technology Co., Ltd.

2.4. Culture Experiments of N Transformation

2.4.1. Flow Culture Experiments to Determine Denitrification and Anammox Rates

At each sampling time, the three sediment cores in the tailored plexiglass tubes were used for flow culture to determine the denitrification and anammox rates in the sediments, as shown in Figure S4a in Supporting Information S1 (Xu et al., 2009). Two nozzles at the top of each plexiglass tube connected the inflow and outflow containers. The inflow was the untreated in situ water injected with isotope $^{15}\text{NO}_3^-\text{-N}$, which was pumped to the tube through a peristaltic pump at a flow rate of 1 mL min^{-1} . The water samples in the inflow container before and after the addition of isotopes were collected and filtered (0.45 μm) to analyze the relative abundance of $^{15}\text{NO}_3^-\text{-N}$. Culturing was performed for 24 hr under constant temperature in dark conditions, and samples of outflow water before and after culturing were collected with headspace sampling bottles. The bottles were immediately injected with 0.2 mL of 50% ZnCl_2 solution to fix the nutrients for the analyses of N_2 isotopes to quantify the magnitude of denitrification and anammox. The N isotopes were examined through a membrane inlet mass spectrometer (Swagelok, OH, USA) with a 0.05 $\mu\text{mol L}^{-1}$ detection limit for N_2 .

The denitrification and anammox rates in the sediments were calculated through the following isotope-pairing techniques (Dähnke & Thamdrup, 2013; Thamdrup & Dalsgaard, 2002):

$$\epsilon = [(\text{NO}_3^-)_a - (\text{NO}_3^-)_b] \cdot (\text{NO}_3^-)^{-1} \quad (1)$$

$$r_n = (C_n - C_{n,0}) \cdot \nu \cdot S^{-1} \times 60 \times 24 \quad (2)$$

$$D_S = (D_{15} + D_{14}) - D_{15} \cdot \epsilon^{-1} \quad (3)$$

$$D_w = D_{15} \cdot \epsilon^{-1} \cdot (1 - \epsilon) \quad (4)$$

$$A_{28} = [r_{29} + 2(1 - \epsilon^{-1}) \cdot r_{30}] \cdot \epsilon \cdot (1 - \epsilon) \quad (5)$$

where ϵ is the relative abundance of $^{15}\text{NO}_3^-$ -N (-); a and b indicate the statuses after and before the addition of isotope, respectively; r_n is the release rate of N_2 with different molecular weights ($\mu\text{mol m}^{-2} \text{hr}^{-1}$); C_n and $C_{n,0}$ are the concentrations of N_2 with different molecular weights in the outflow before and after culture ($\mu\text{mol L}^{-1}$), respectively; v is the flow rate regulated by the peristaltic pump (mL min^{-1}); S is the sediment–water contact area in the columnar sample (m^{-2}); D_{15} ($= r_{29} + 2r_{30}$) and D_{14} ($= D_{15} \cdot r_{29}/2r_{30}$) are the denitrification amounts using $^{15}\text{NO}_3^-$ -N and $^{14}\text{NO}_3^-$ -N ($\mu\text{mol m}^{-2} \text{hr}^{-1}$), respectively; D_s is the denitrification rate of nitrate from the sediment ($\mu\text{mol m}^{-2} \text{hr}^{-1}$); D_w is the denitrification rate of nitrate from overlying water ($\mu\text{mol m}^{-2} \text{hr}^{-1}$); and A_{28} is the $^{28}\text{N}_2$ flux generated during anammox ($\mu\text{mol m}^{-2} \text{hr}^{-1}$).

2.4.2. Static Culture Experiments to Determine N Mineralization and Nitrification Rates

The surface sediments in the 12 PVC pipes mentioned above were used for static culture to determine the net N mineralization and nitrification rates in the sediments, as shown in Figure S4b in Supporting Information S1 (Seeley et al., 2020). For sediments collected during DPs, 3 of the 12 PVC pipes were mixed into one sample, from which sediment NH_4^+ -N and NO_3^- -N contents were determined on day 0 of the experiment. The remainder of the PVC pipes were placed in a fume hood and under light for culture. Distilled water was added to the sediments during culture to maintain their moisture content, and the temperature was adjusted to mimic the in situ temperature. On the 3rd, 7th, and 15th days of culture, each of the three culture pipes was taken to determine the sediment NH_4^+ -N and NO_3^- -N contents. Once the sediment in a pipe was analyzed, it was not returned for further culture. Sediments collected during FPs were covered by in situ water, and the upper part of the pipes was sealed with water-retaining, breathable membranes with holes for ventilation.

The net N mineralization and nitrification rates in the sediments were calculated via the change in NH_4^+ -N and NO_3^- -N (Worsfold et al., 2008):

$$M_{\text{net}} = \frac{(\text{NH}_4^+ + \text{NO}_3^-)_b - (\text{NH}_4^+ + \text{NO}_3^-)_a}{T} \quad (6)$$

$$N_{\text{net}} = \frac{(\text{NO}_3^-)_b - (\text{NO}_3^-)_a}{T} \quad (7)$$

where M_{net} and N_{net} are the net N mineralization rate and net nitrification rate ($\text{mg kg}^{-1} \text{d}^{-1}$), respectively; $(\text{NH}_4^+ + \text{NO}_3^-)_a$ and $(\text{NH}_4^+ + \text{NO}_3^-)_b$ are the total contents of NH_4^+ -N and NO_3^- -N (mg kg^{-1}) in the sediment before and after culture, respectively; $(\text{NO}_3^-)_a$ and $(\text{NO}_3^-)_b$ are the contents of NO_3^- -N (mg kg^{-1}) in the sediment before and after culture, respectively; and T is the culture time (d).

2.5. Quantification of N Flux and Budget

2.5.1. Release Tests to Determine N Release Fluxes in Sediments

At each sampling time, the three other treated sediment cores were used to determine the release fluxes of NH_4^+ -N, NO_3^- -N, and TN in the sediments, as shown in Figure S4c in Supporting Information S1 (Fan et al., 2002). Prior to culturing, the original overlying water of all samples was replaced with the same volume of filtered in situ water, and the liquid level was marked on the plexiglass tubes. All the samples were cultured under in situ temperature in the dark. At 0, 12, 24, 36, 48, and 72 hr, 50 mL of water was collected at 5 cm above the sediment with a pipette. After each collection, each sample was slowly injected with filtered in situ water to maintain the water balance.

The release fluxes of N species (NH_4^+ -N, NO_3^- -N, and TN) from the sediments to the overlying water were calculated as follows:

$$f_i = \left[V \times (C_0 - C_n) + \sum_{i=1}^n V_{i-1} \times (C_a - C_{i-1}) \right] / (S \times t) / 1000, \quad (8)$$

where f_i is the average release flux ($\text{g m}^{-2} \text{d}^{-1}$). A negative value indicates the release of solute from sediment to water, and vice versa; V is the volume of overlying water in the columnar sample (L); C_n , C_0 , and C_{i-1} are the mass concentrations of a substance at the n th, 0th (initial), and $i-1$ th sampling (mg L^{-1}), respectively; C_a is the

mass concentration of the substance in the added water sample (mg L^{-1}); V_{i-1} is the volume of overlying water at the $i-1$ th sampling (L); S is the cross-sectional area of the columnar sample (m^2); and t is the time (d).

The release fluxes of the N species per meter along the flow direction were calculated as follows:

$$F_i = f_i \times \frac{h - h_0}{\sin \gamma}, \quad (9)$$

where F_i is the release flux per meter along the flow direction ($\text{g m}^{-1} \text{d}^{-1}$); h_0 and h are the initial and instant water levels (m), respectively; and γ is the average slope of the DA ($^\circ$).

Furthermore, the continuous change in F_i , denoted as $F_i(t)$, throughout a complete hydrological cycle can be estimated as follows:

$$F_i(t) = f_i(t) \times \frac{h(t) - h_0}{\sin \gamma}, \quad (10)$$

where $f_i(t)$ represents the interpolation of the 8 release fluxes (obtained from the 8 sampling times) throughout the year ($\text{g m}^{-2} \text{d}^{-1}$); and $h(t)$ is the time series of the water level (m).

2.5.2. Modeling of N Exchange Flux Between Sediment and Overlying Water

The only fluxes in the DA's mass balance that we were unable to determine using the measured field and experimental data were the exchange fluxes for each N species across the sediment-water interface. Therefore, we applied a 2D flow and reactive transport model to estimate $\text{NH}_4^+\text{-N}$, $\text{NO}_3^-\text{-N}$, and TDN exchange at the sediment-water interface during water level fluctuation. The formulation, calibration, and validation of the numerical model were conducted using measured temperature, N concentration, and DO data for both overlying water and pore water, described in detail in Texts S2 and S3 in Supporting Information S1. Within the model, the chemical reaction module has coupled the effects of temperature and DO on the microbial-mediated coefficients of nitrification and denitrification (U_{NI} and U_{DN}) (Text S3.2 in Supporting Information S1).

By applying the model, the exchange fluxes of the N species ($\text{NH}_4^+\text{-N}$, $\text{NO}_3^-\text{-N}$, and TDN) per meter along the flow direction were calculated as follows:

$$J_i(t) = \int_0^l v_n(l,t) \cdot C_i(l,t) dl, \quad (11)$$

where J_i is the exchange flux ($\text{g m}^{-1} \text{d}^{-1}$). A positive value indicates that the overlying water infiltrates into the sediment, and vice versa. l is the length of the sediment-water interface (m); $v_n(l,t)$ is the normal flow velocity along the sediment-water interface (m s^{-1}); and $C_i(l,t)$ is the concentration of solute i along the sediment-water interface (mg L^{-1}).

2.5.3. Annual Budget of Net TN Load From DA to Water Column

The annual release load of TN per meter along the flow direction (M_1 , g m^{-1}) was calculated as follows:

$$M_1 = \int_0^T F_{\text{TN}}(t) dt, \quad (12)$$

where T is a full hydrological cycle (d); and $F_{\text{TN}}(t)$ is the release flux of TN (Equation 10). A negative value indicates the release of solute from sediment to water, and vice versa.

The annual exchange load of TN (i.e., TDN) per meter along the flow direction (M_2 , g m^{-1}) was calculated as follows:

$$M_2 = \int_0^T J_{\text{TDN}}(t) dt, \quad (13)$$

where T is a full hydrological cycle (d); and J_{TDN} is the exchange flux of the TDN (Equation 11). A positive J_{TDN} indicates that the overlying water infiltrates into the sediment, and vice versa.

In general, within a full hydrological cycle, a portion of the exchange load (i.e., infiltration minus exfiltration) is retained in the DA, while the other portion is removed through denitrification. The calculation for the latter is as follows:

$$M_{\text{DN}} = \int_0^T \int_{\Omega} \theta R_i d\Omega dt, \quad (14)$$

where M_{DN} is the total mass of nitrate being removed from denitrification (g m^{-1}); R_i is the reaction rate for $\text{NO}_3^- - \text{N}$ ($\text{mg L}^{-1} \text{d}^{-1}$); Ω is the simulation area (m^2); and θ is the water content of the sediment (–).

Overall, the annual budget of the net TN load from the DA to the water column (ΔM , g m^{-1}) was calculated as follows:

$$\Delta M = M_1 + M_2 \quad (15)$$

A positive ΔM indicates the DA is an N sink, and vice versa.

2.6. Statistical Analyses

The study utilized Pearson correlation analysis to determine the correlation between experimental indicators and influencing factors, specifically N transformation rates, N species, microbial abundances, water level, temperature, DO, ORP, and TOC (DOC), with a p -value of 0.05. All statistical analyses were performed using SPSS v22 (SPSS Inc., North Chicago, IL, USA). To address model uncertainty, Monte Carlo simulation and Latin hypercube sampling were employed in Matlab 2018b (MathWorks Inc., Massachusetts, USA) (see Text S4 in Supporting Information S1 for details).

3. Results

The essential results at the GY site are presented in detail here, while the comparative spatial study of the three sites is shown in the Supporting Information (Text S1 in Supporting Information S1).

3.1. Dynamics of Physical and Chemical Properties in the DA

The water level of the TGR varied profoundly with the season, with especially high water levels in dry seasons and low levels in wet seasons (Figure 2a). During the LWP, the DA was exposed to hot weather (Figure 2b), providing better conditions for the growth of hygrophilic herbs (Figure 1). From May to July, the overlying water turbidity was high, and the TSS level was approximately 12 times higher than that in other months (Figure 2c). The pattern in chlorophyll-a concentrations corresponded to the changes in water temperature (Figure 2d), except in March when a phytoplankton bloom occurred when temperature was minimized. The DO concentration at the sediment–water interface was generally stable in the LWP except during brief periods of intermittent inundation around July (Figure 2e). DO sharply decreased in the early FP before a gradual recovery. The DO level decreased slightly in the HWP and then rebounded during the DP before declining steeply with the onset of rain in May. Figure 2f shows the overlying water ORP was invariably negative with greater reducibility at high water levels and less at low water levels, which showed a positive correlation with DO (Figure S5a in Supporting Information S1).

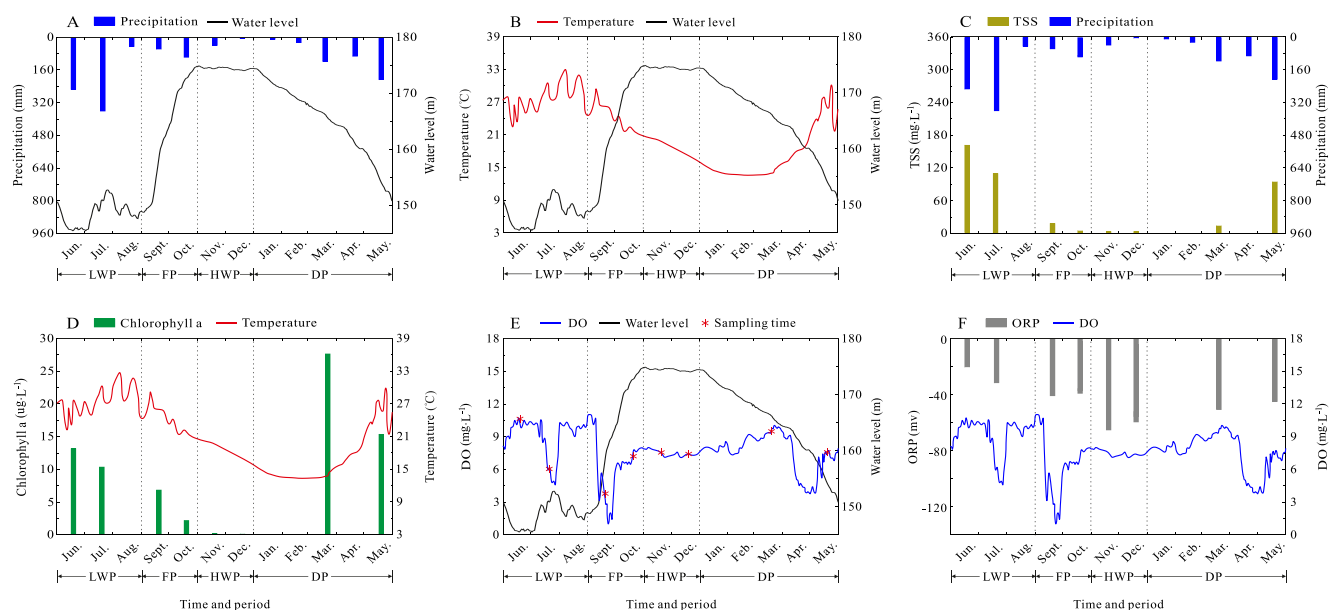


Figure 2. Changes in the basic physical and chemical properties in the reservoir drawdown area (average from 2018 to 2020). (a) Precipitation versus water level; (b) overlying water temperature versus water level; (c) average total suspended solids (TSS) concentration of overlying water versus precipitation; (d) average chlorophyll-a concentration of water profile versus temperature; (e) overlying water dissolved oxygen (DO) concentration versus water level; and (f) overlying water oxido-reducing potential (ORP) versus DO concentration. LWP, low-water-level period; FP, flooding period; HWP, high-water-level period; and DP, drying period.

3.2. Dynamics of N Functional Microorganisms in the DA

Various microbial abundances in the sediment exhibited significant correlations with each other, with a median r of 0.69 ($p = 0.021$), as shown in Table S3 in Supporting Information S1. The abundances of *nirS* and *ureC* were much higher than those of *hzsB* and *AOB* (Figure 3). Sediment inundation had a negative effect on most microorganisms (median $r = -0.40$, $p = 0.015$), and they maintained a low level or gradual decrease in abundance during flooding and then recovered during drying. The Pearson correlation analysis, detailed in Table S3 in Supporting Information S1, further uncovered the robust correlations between water temperature and microbial abundances (median $r = 0.65$, $p = 0.020$), followed by total organic carbon (median $r = 0.42$, $p = 0.034$). Ambient DO had a positive effect on the abundances of sediment *ureC* and *AOB*, whereas ORP had a negative effect on those of *nirS* and *hzsB*.

3.3. N Species Dynamics and Transformation Rates in the DA

DIN in the overlying water at all sampling times was primarily in the form of NO_3^- -N, which accounted for 88%–97% of TN (Figure 4a). During the LWP, the water DIN concentration showed a decreasing trend. DIN concentration (from 1.32 mg L^{-1} to 1.25 mg L^{-1} , $\text{GR\% (growth rate)} = \frac{(\text{Sample size}-1)\sqrt{1.25/1.32} - 1}{1} = -1.8\%$) slightly declined in the FP and HWP. During the DP, the aquatic N species concentrations changed substantially in different directions: from January to March, the ON concentrations increased sharply from 0.56 mg L^{-1} to 1.04 mg L^{-1} ($\text{GR\%} = 36.3\%$), whereas that of NO_3^- -N decreased from 0.99 mg L^{-1} to 0.52 mg L^{-1} ($\text{GR\%} = -27.5\%$). From March to May, the TN and NO_3^- -N concentrations increased considerably from 1.63 mg L^{-1} to 2.21 mg L^{-1} ($\text{GR\%} = 16.4\%$) and from 0.52 mg L^{-1} to 1.09 mg L^{-1} ($\text{GR\%} = 44.8\%$), respectively. In the sediment, TN was primarily present in the form of ON, and the pattern of change in both forms aligned consistently (Figure 4b). Taking ON as an example, its content increased by over 50% from 480 mg kg^{-1} to 800 mg kg^{-1} ($\text{GR\%} = 18.6\%$) in the LWP and early FP (June to September) before increasing slightly from 800 mg kg^{-1} to 807 mg kg^{-1} ($\text{GR\%} < 1\%$) afterward (October to May). The sediment IN varied greatly in each period. During the LWP and FP, the sediment IN was primarily NH_4^+ -N, whose content increased gradually and peaked in October; conversely, the sediment NO_3^- -N initially increased and then decreased. In the HWP and DP, the sediment IN was mostly NO_3^- -N, whose content initially decreased and then increased; the sediment NH_4^+ -N showed the same pattern of change.

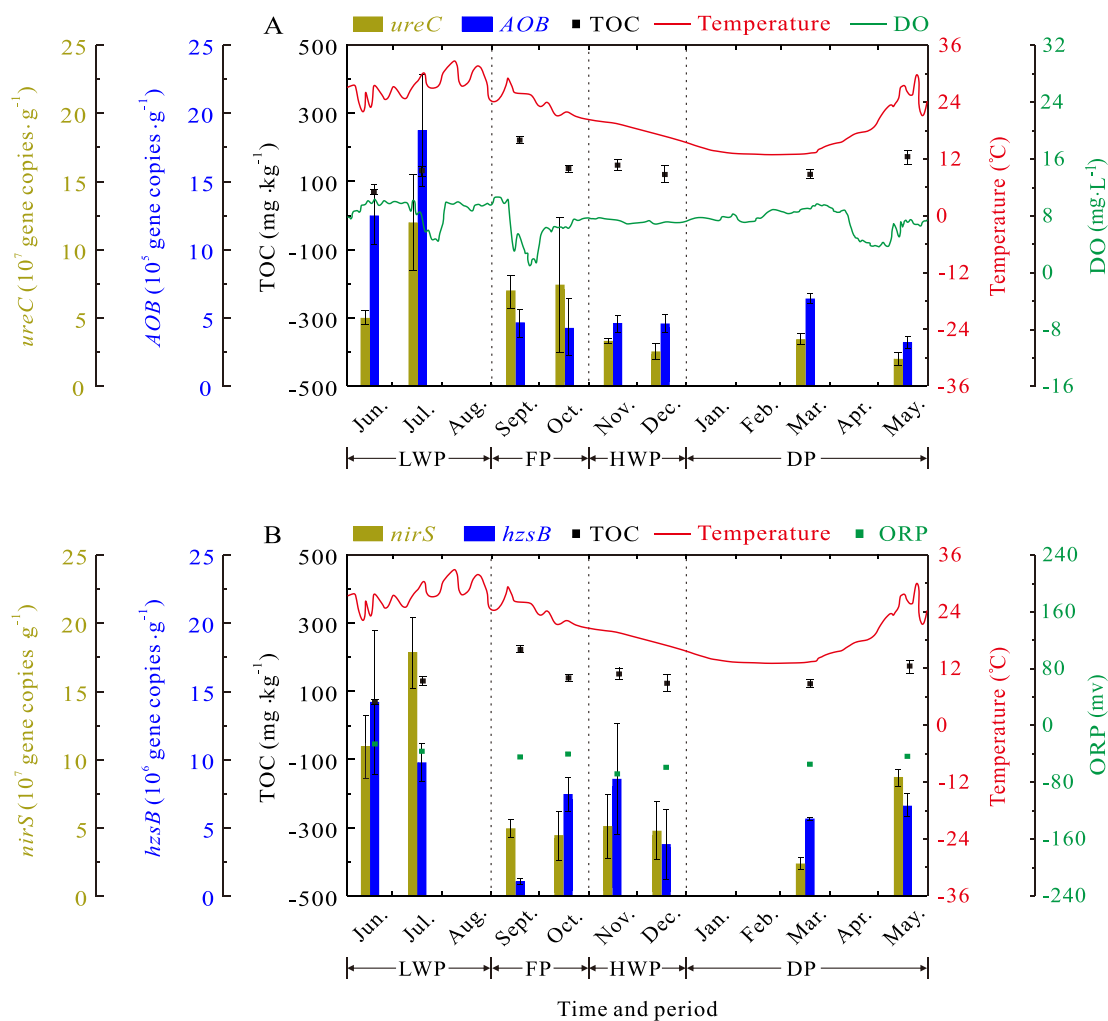


Figure 3. Changes in (a) aerobic microbial abundance (mineralizing gene [*ureC*], nitrifying gene [*AOB*]) and (b) anaerobic microbial abundance (denitrifying gene [*nirS*], anammox gene [*hzsB*]) in the reservoir drawdown area (average from 2018 to 2020). Error bars indicate standard deviations for six detection values in 2 years (excluding outliers). TOC, total organic carbon; DO, dissolved oxygen; ORP, oxido-reduction potential; LWP, low-water-level period; FP, flooding period; HWP, high-water-level period; and DP, drying period.

The capacities of N mineralization and nitrification in the sediment, determined by the static culture experiments, initially increased and then decreased in the LWP and FP (Figure 4c). The net N mineralization and nitrification rates in the sediment became negative during the HWP and then somewhat recovered during the DP. The rates of sediment denitrification and anammox, determined by the flow culture experiments, were high during the HWP and the late stage of the DP, and peaked in May. N removal in the sediment depended primarily on denitrification, and anammox accounted for <5% of the total removal (Figure 4d). Pearson correlation analysis (Table S4 in Supporting Information S1) showed that sediment N mineralization and nitrification were primarily driven by *ureC* and *AOB* abundances ($r = 0.74, 0.54; p = 0.025$). Ambient ORP (or DO), instead of microbial abundance, was the main factor affecting sediment denitrification ($r = 0.71, p = 0.010$) and anammox ($r = 0.32, p = 0.023$).

3.4. N Dynamics Over a Complete Hydrological Cycle in the DA

TN exhibited a release from the DA to the water column that peaked during the LWP (Figure 5a). The release fluxes of N species escalated with the reservoir impoundment (within FP), reaching their maximum before the end of HWP. Specifically, NO_3^- -N mainly diffused from the water to the sediment, whereas NH_4^+ -N and ON exhibited the opposite trend, moving from the sediment to the water column, leading to a reversal of the TN release direction from FP to HWP. During reservoir discharge (within DP), TN release was high, echoing a pattern similar to that of ON, attaining a large negative peak in March (Figure 5a). Figure 5b depicts the modeled

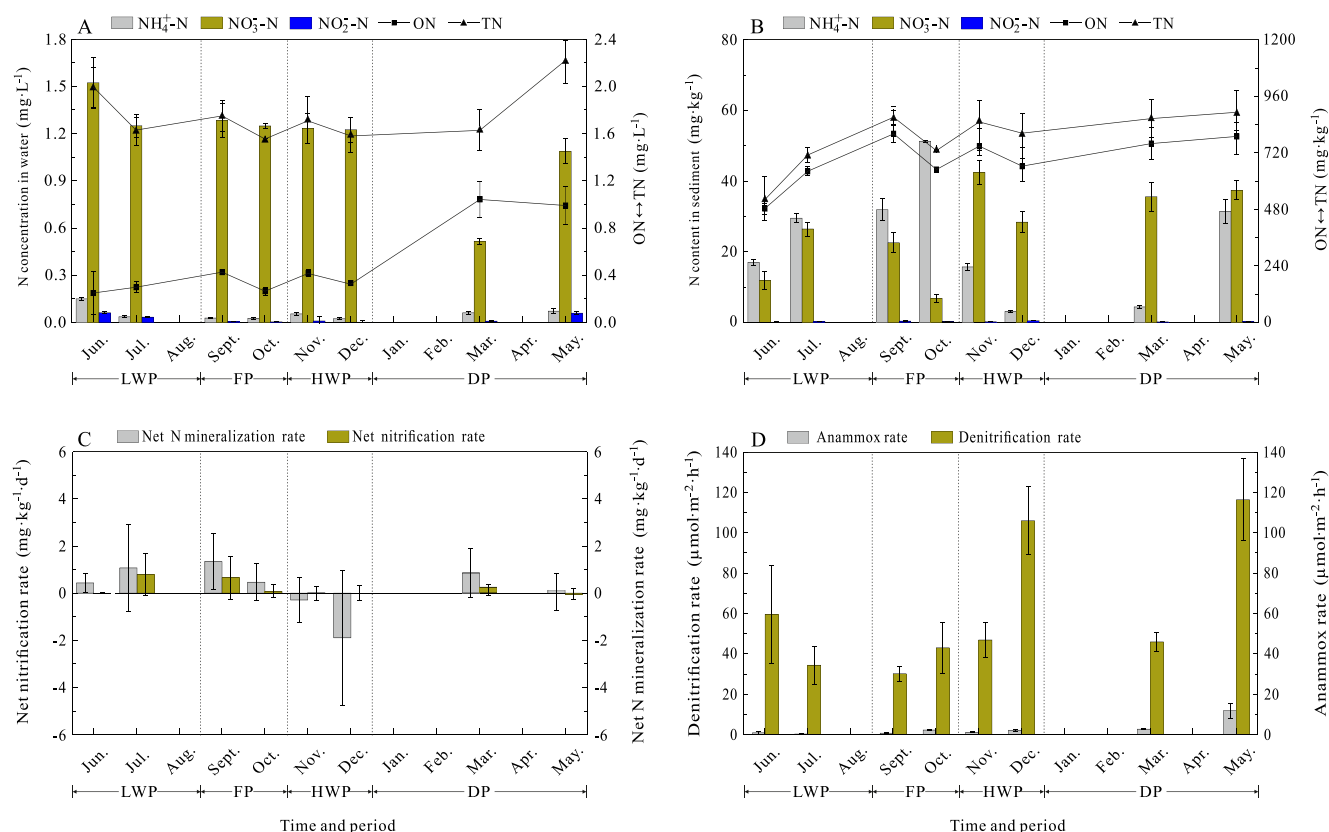


Figure 4. Changes in N species and transformation rates in the reservoir drawdown area (average from 2018 to 2020). (a) Concentrations of N species in the overlying water; (b) contents of N species in the sediment; (c) net N mineralization and nitrification rates in the sediment determined by the static culture experiments; and (d) denitrification and anammox rates in the sediment determined by the flow culture experiments. Error bars indicate standard deviations for six detection values in 2 years (excluding outliers). LWP, low-water-level period; FP, flooding period; HWP, high-water-level period; and DP, drying period.

exchange fluxes of N species between the DA and the water column. The infiltration of TDN into the sediment mainly occurred in the FP and HWP, whereas the exfiltration of TDN primarily took place during the DP. Notably, the peak of NO_3^- -N infiltration was larger and occurred later (late December) than that of NH_4^+ -N, whereas its peak in exfiltration was smaller and occurred earlier (mid-January).

4. Discussion

4.1. Hydrological Mechanisms Associated With N Cycling

Past research has shown that sedimentation in flood control reservoirs is high during wet seasons, which correspond with the low-water period (LWP), due to large TSS fluxes being loaded to aquatic systems from enhanced terrestrial runoff (Figure 6a), which in turn stimulates coupled nitrification–denitrification in the water column as high TSS concentrations (Figure 2c) provide sites for these reactions to occur (Liu et al., 2013; Xia et al., 2016; Yao et al., 2016). In our results, we similarly found that the concentration of NO_2^- -N (an intermediate in denitrification) in the water was positively correlated with that of TSS (Figure S5b in Supporting Information S1), indicating enhanced denitrification during periods of high TSS transport and sedimentation. Evidence for higher water column coupled nitrification–denitrification during the wet season was further supported by decreases in the concentrations of NH_4^+ -N and NO_3^- -N (Figure 4a), suggesting that the water column is a metabolizing dissolved N species and removes them from the atmosphere during the inundation periods. On the other hand, during these inundation periods, the DA sediment itself provides an ideal habitat for the proliferation of aerobic microorganisms because the stress caused by the alternating cycles of wetting and drying increases the organic N content and pH levels in the sediment (Guo et al., 2016; Ye et al., 2017), thereby enhancing the sediment N mineralization and nitrification rates (Text S5 in Supporting Information S1). Thus, when considering these enhanced mineralization and nitrification rates plus rainfall inputs, the contents of ON,

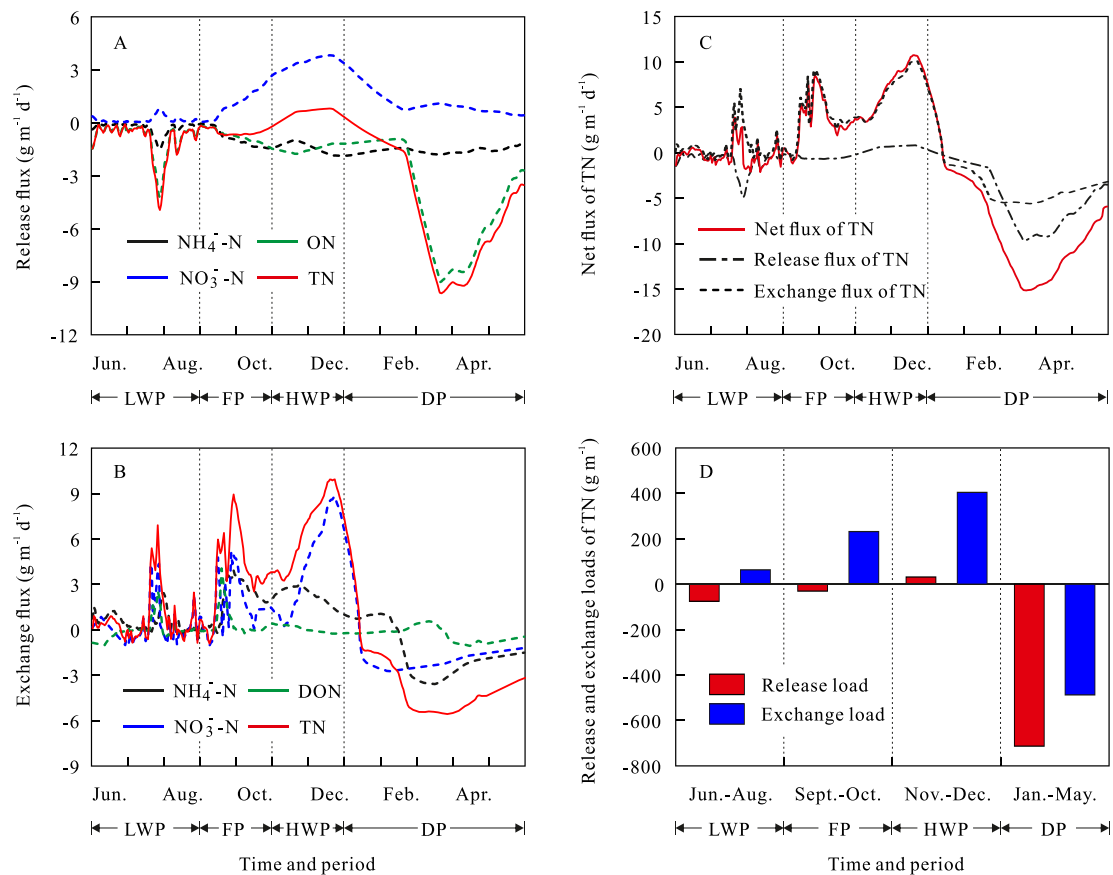


Figure 5. Dynamics of N flux and budget (per meter along the flow direction) at the sediment–water interface of the drawdown area (average from 2018 to 2020). A positive value indicates that the drawdown area is an N sink, and vice versa. (a) Annual variation of release fluxes of N species (Equation 10); (b) annual variation of model-derived exchange fluxes of N species (Equation 11); (c) release, exchange, and net fluxes of TN; and (d) release and exchange loads of TN (Equations 12 and 13). Smoothing treatment on all the curves is achieved by using the FFT smoothing function of Origin software. LWP, low-water-level period; FP, flooding period; HWP, high-water-level period; and DP, drying period.

$\text{NH}_4^+\text{-N}$, and $\text{NO}_3^-\text{-N}$ in the sediment increase (Figure 4b), making the DA sediment a dissolved N source to the water during this period (Yu et al., 2020). Despite this N release, the TN in the overlying water does not increase correspondingly, given that the water column itself possesses a robust N removal capacity via coupled nitrification–denitrification.

During the flooding period (FP) in September and October, the inundation of the DA triggers the release of N into the reservoir's water column (Figure 6a) (Lu et al., 2017). However, the DIN concentration in the overlying water remained largely stable throughout the period (Figure 4a). This stability can be mainly attributed to dilution from the surge in water volume (Xiang et al., 2021a). In the sediment, the overall extent of N mineralization declines with the decreasing temperature (Text S5 in Supporting Information S1), but stabilizes around $1 \text{ mg kg}^{-1} \text{ d}^{-1}$. Accordingly, sediment $\text{NH}_4^+\text{-N}$ increases during this period due to the consumption of ON (Pan et al., 2008). Additionally, the rapid increase in water depth causes a significant decline in DO as the solubility of DO decreases under high water pressure, thereby weakening nitrification (Stordy et al., 2004). This may further contribute to the temporary accumulation of $\text{NH}_4^+\text{-N}$ in the sediment (Figure 4b). Conversely, the rising water level and associated drop in DO enhance denitrification, leading to a short-term decline in $\text{NO}_3^-\text{-N}$ within the sediment.

The reservoir maintains its highest water level in winter with high water transparency (i.e., low TSS) (Figure 6a). The release of N nutrients from the sediment is limited (Figure 5) (Pan et al., 2008) due to the reduced mineralization, which is suppressed by the low temperature. Conversely, the transfer of DIN from the water column to the sediment is large (Figure 5c) due to the high water pressure (Kang et al., 2024). This shift, combined with the low potential for coupled nitrification–denitrification, controlled by the low TSS concentrations (Figure 2c), maintains relatively stable concentrations of DIN and ON in the overlying water. Within the sediment,

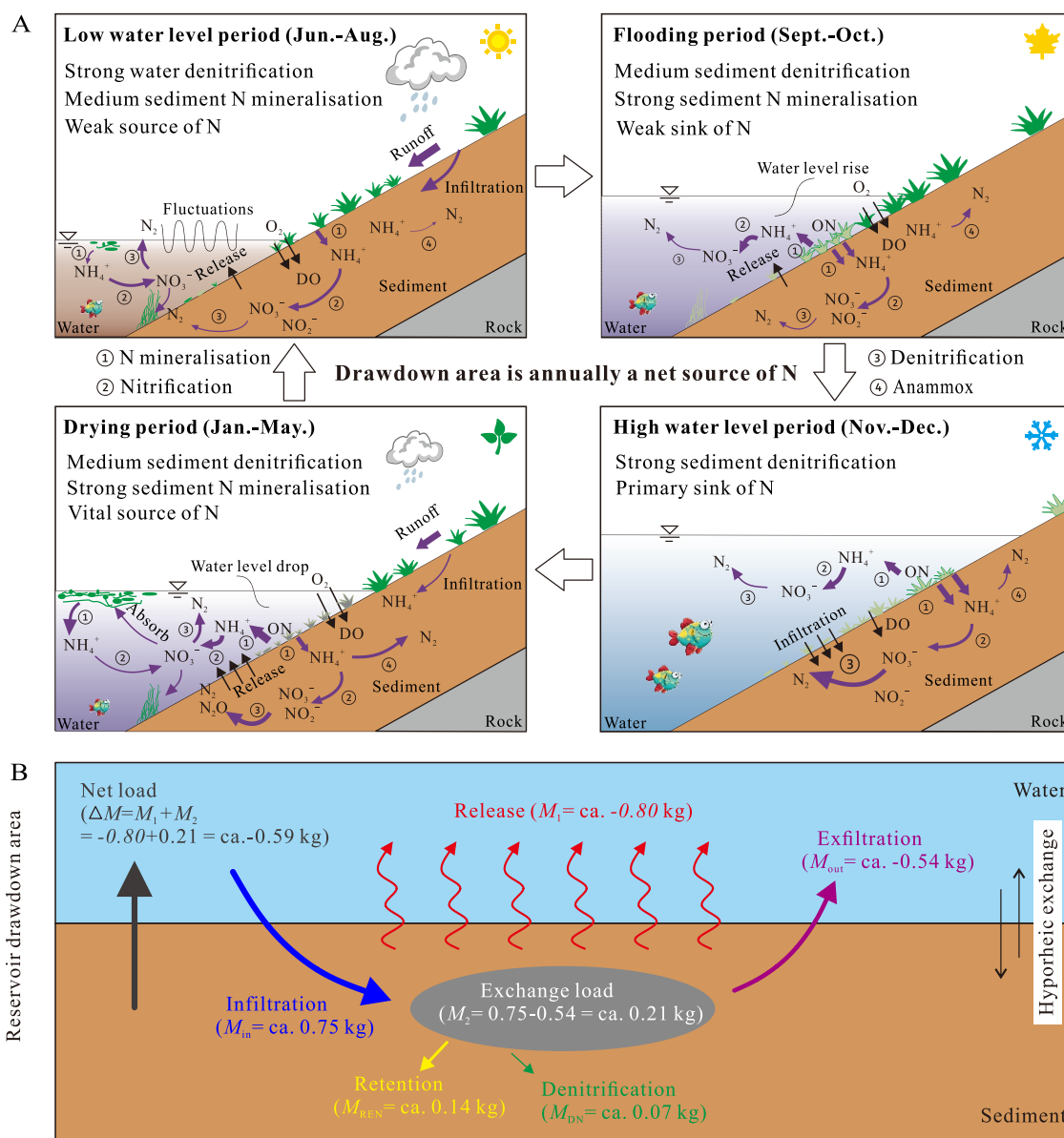


Figure 6. Conceptual mechanism of N cycling and TN mass balance in the reservoir drawdown area. (a) Conceptual mechanism of N cycling; and (b) TN mass balance in the reservoir drawdown area. Each number represents the total yearly load for the DA per meter along the flow direction. The italicized numbers denote the load from the field tests (Section 2.5.1), while other normally formatted numbers represent the loads from the model (Section 2.5.2). A positive value indicates the DA is an N sink, and vice versa.

considerable amounts of residual $\text{NH}_4^+\text{-N}$ from earlier periods undergo nitrification into $\text{NO}_3^-\text{-N}$. Nevertheless, both the concentrations of $\text{NH}_4^+\text{-N}$ and $\text{NO}_3^-\text{-N}$ decrease in this period, which is attributed to the significant enhancement in denitrification and anammox (Figure 4d) that is mainly driven by the low ORP (Text S5 in Supporting Information S1) (Xia et al., 2016).

During the drying period (DP) in the spring, elevated nutrient concentrations and a temperature increase trigger a phytoplankton bloom in March (Figure 6a) (Li et al., 2012). The phytoplankton takes up N nutrients and reduces the water $\text{NO}_3^-\text{-N}$ concentration considerably (Figure 4a). Conversely, sediment ON and TN increase due to the death and deposition of phytoplankton (Chen et al., 2020). Meanwhile, with the recovery of microbial abundance, the buried ON (a combination of dead phytoplankton deposition and previously submerged plant residues) undergoes substantial consumption through enhanced N mineralization and nitrification (Pan et al., 2008), causing an increase in $\text{NH}_4^+\text{-N}$ and $\text{NO}_3^-\text{-N}$ in the sediment in March. However, by May, the phytoplankton population

and the water's ON concentration decreased because of hydrodynamic disturbance (Liu et al., 2012). Despite this decrease, the overlying water's TN concentration exceeded that in March (2.2 mg L^{-1}) (Figure 4a). Moreover, sediment DIN sharply increased from March to May (Figure 4b) despite denitrification and anammox rates peaking in May. Together with the rainfall patterns, these findings lead us to conclude that the increase in sediment and water N in May is caused by nonpoint source pollution from the DA (Xiang et al., 2021b).

4.2. N Budget of Reservoir DA and Ecological Implications

Over a complete hydrological cycle, the DA per meter along the flow direction releases ca. 0.80 kg of TN to the water column, while its removal load of TN (infiltration minus exfiltration) is ca. 0.21 kg (Figure 6b). Within this removal load, ca. 0.07 kg is removed through sediment denitrification, and ca. 0.14 kg is retained within the sediment. Consequently, the DA per meter along the flow direction releases a net TN load of ca. 0.59 kg ($\Delta M = 0.80 - 0.21 \text{ kg}$) to the reservoir annually. The model-based result of 0.59 kg has demonstrated low uncertainty: the 90% confidence interval of the simulated ΔM from Latin-hypercube samples fell between 581 and 593 g, with an average of 588 g, closely aligning with the ca. 0.59 kg derived from the deterministic model (Text S4 in Supporting Information S1). Furthermore, the changes in N species derived from the model exhibit good consistency with the mean values based on Latin-hypercube samples, as detailed in Text S4 in Supporting Information S1. Additionally, the credibility of the model-derived ca. 0.59 kg is supported through comparison with findings from other similar studies (Text S6 in Supporting Information S1).

N release primarily originates from the degradation of plants (Chang & Wen, 1997; Chen et al., 2019; Xiao et al., 2017), and this process mainly occurs during the drying period around March (Figure 5d). Before March, the complete hydrolysis of plants is hindered (Pan et al., 2008); however, as temperature warms during drying, the degradation of previously buried ON is facilitated, causing a large amount of N to escape under the decreasing water pressure. Our result of ca. 0.80 kg m^{-1} aligns well with a prior study by Xiao et al. (2017), where an annual TN load of 81.1 kg ha^{-1} resulted from plant decomposition in the TGR's DA. This parallel finding reinforces the robustness of our findings.

TN sequestration pathways, on the other hand, are not dominated by a single process. TN loads possibly originating from the release of DA or from the reservoir water itself re-enter the sediment during water level fluctuations, undergoing processes such as advective transport, redox reactions (e.g., nitrification and denitrification), and retention (Jiang et al., 2022). Our model results indicated that sediment denitrification removes ca. 0.07 kg m^{-1} of the TN loaded back into the sediment annually, with an N removal efficiency of 9.6% (Text S6 in Supporting Information S1), which is comparable to that of other studies on riparian and hyporheic zones (e.g., Shuai et al., 2017). The transport of the retained N (ca. 0.14 kg m^{-1}) to the groundwater is unlikely due to the impervious nature of some reservoirs or the use of impermeable curtains to ensure storage capacities. In the TGR, the thickness of the permeable sediment in the DA is approximately 55 cm. Instead, some of the retained N may escape into the atmosphere via biochemical reactions upon exposure of the DA during drying (Keller et al., 2021; Shi et al., 2021). Additionally, a portion of the retained N may be absorbed by plants in the following year (Zhou et al., 2014), subsequently releasing it back into the reservoir, thus repeating an internal circulation process within the DA. Consequently, plant harvesting can effectively assist in removing this N fraction from the reservoir, thereby mitigating its accumulation. In recent years, the Chinese government has imposed a range of policies for managing drawdown areas, such as garbage clearance and prohibition of all human activities, aimed at safeguarding the water quality of reservoirs (Li et al., 2019). However, they overlooked the pruning of dense herbaceous plants that grow in situ seasonally (Figure 1), and in this study, we provide evidence and underscore the necessity of expanding this initiative.

Although the DA has a purifying effect on the reservoir's N water quality, the net release of TN load means it contributes to the accumulation of N in the reservoir. The backflow of the mainstream density current is typically considered the primary factor leading to eutrophication in the TGR tributaries (Li et al., 2020; Liu et al., 2012). According to Hu et al. (2012), the estimated annual TN load from the mainstream of the TGR to the Pengxi River is ca. 0.90 kg m^{-1} , which is on the same order of magnitude as the net release load of TN from the DA (ca. $0.59 \text{ kg m}^{-1} \text{ year}^{-1}$) (Figure 6b). The influence of the mainstream density current on tributaries usually fades further upstream. Hence, a spatial boundary exists for the influence of density current on the eutrophication of a tributary (Figure S6 in Supporting Information S1). For example, the GY site is located in the backwater end of the Pengxi River, where the influence of the mainstream density current is low (Figure S6

in Supporting Information S1). Thus, the algal blooms observed here can be presumed mainly to be driven by sediment release (Wang et al., 2022). This suggests that the peak release flux of TN from the DA at the GY site in March (Figure 5a) is likely responsible for the observed algal blooms (Figure 2d) in the reservoir bay. Eutrophication in the reach from the spatial boundary to the estuary is likely primarily caused by the mainstream density current, whereas eutrophication beyond this boundary is more attributed to the DA's release. Therefore, this study represents the first quantitative documentation of reservoir DAs as suppliers of N to the water column at a magnitude that is comparable to the load carried by the mainstream density current. These findings indicate that the role of DAs cannot be neglected when managing the prevention and control of eutrophication in reservoir tributaries.

4.3. Regional and Global Significance

Flood control reservoirs such as the TGR are widely distributed in North America, Asia, and Europe (Zhang & Gu, 2023). In China, reservoirs with flood control as one of their functions account for approximately 30% of the total number of reservoirs (Table S5 in Supporting Information S1). During wet seasons, this type of reservoir maintains a low water level, exposing extensive DAs that provide favorable conditions for the growth of massive plants (Bao et al., 2015). These plants absorb N from sediments (a combination of internally retained N and externally deposited N) and incorporate it into their biomass (Lv et al., 2019; Z. Wang et al., 2019), and become a source of easily released N during subsequent dry seasons (Chen et al., 2019; Xiao et al., 2017). Our findings have clarified the source-sink transition of N between the DA and the reservoir, and we have quantified the annual net release load of TN from a DA to the reservoir water column (ca. 0.59 kg m^{-1}). The total inundation area of reservoirs in China is estimated to be over $50,000 \text{ km}^2$ (Song et al., 2022). Assuming that an average of 15% of the total reservoir inundation area is anti-seasonally drawn down, as estimated globally by Keller et al. (2021) using satellite imagery, the total Chinese flood control reservoir DA is approximately $7,513 \text{ km}^2$ (Table S6 in Supporting Information S1). If we assume our annual estimate of 0.59 kg m^{-1} is representative of net release from all Chinese reservoir DAs, a net flux of over 44,300 t of N is mobilized to the water column annually in Chinese watersheds and potentially delivered to coastal zones (Table S6 in Supporting Information S1). To put this in context, the annual TN load from rivers delivered to coastal zones in China is estimated to be $2.5 \times 10^6 \text{ t}$ (Qu & Kroeze, 2010); this indicates that approximately 2% of all N delivered to Chinese coastal waters from river networks originates from DA release. The N load released by reservoir DAs is mainly discharged downstream in spring, which may contribute to phytoplankton blooms in estuaries and coastal zones, and potentially, ocean hypoxia or harmful algal bloom scenarios (Breitburg et al., 2018). Therefore, sustainable harvesting of plants in DAs prior to submergence should be considered as an effective measure to indirectly remove both internal and external sources of N in DAs, which is of great significance in reducing N accumulation in reservoirs and preventing eutrophication in both the reservoirs themselves and downstream areas.

5. Conclusions

Reservoir DAs have cyclical positive and negative effects on the N quality of the reservoir. Our observation and modeling efforts on the N cycling in the TGR reveal that DA is a net source of N to the reservoir water within a full hydrological cycle, although approximately 30% of the released TN load is eliminated by the sediment through denitrification and capture (most of which escapes into the atmosphere). We use our findings to estimate that Chinese TN mobilized from reservoir DAs represents about 2% of the overall flux of N to Chinese coastal zones annually. We show that N species escape from the DA during drying periods with the recovery of N mineralization and a decrease in water pressure, whereas denitrification in the sediment mostly occurs during the flooding periods. The underlying mechanism dominating the N cycling characteristics in different periods is dam-controlled hydrological processes, specifically rising and falling water levels. Our findings shed light on the environmental effects of DAs on reservoirs and offer a new perspective on accurate measures for preventing reservoir and downstream eutrophication, potentially as far as receiving coastal water bodies.

Data Availability Statement

The source data used for creating the figures in this article are from the authors (Liu, 2023). The global reservoir data are publicly available from the GRanD data set (Zhang & Gu, 2023). The collection of flood control reservoirs in China is available at (Liu, 2022).

Acknowledgments

This work was funded by the National Key Research and Development Program of China (2022YFC3203900), the National Natural Science Foundation of China (52121006, 42207240), and the Natural Science Foundation of Jiangsu Province (BK20200158). Additionally, Qiuwen Chen received support from the XPLOER PRIZE, and Taylor Maavara was supported by an Independent Research Fellowship from the United Kingdom's Natural Environment Research Council (NERC), Grant NE/V014277/1. We extend our heartfelt gratitude to the anonymous reviewers and associate editor for their valuable comments that have significantly improved the overall quality of the manuscript.

References

- Bao, Y., Gao, P., & He, X. (2015). The water-level fluctuation zone of three Gorges reservoir—A unique geomorphological unit. *Earth-Science Reviews*, *150*, 14–24. <https://doi.org/10.1016/j.earscirev.2015.07.005>
- Breitburg, D., Levin, L. A., Oschlies, A., Grégoire, M., Chavez, F. P., Conley, D. J., et al. (2018). Declining oxygen in the global ocean and coastal waters. *Science*, *359*(eaam7240), 1–11. <https://doi.org/10.1126/science.aam7240>
- Brunke, M., & Gonser, T. (1997). The ecological significance of exchange processes between rivers and groundwater. *Freshwater Biology*, *37*(1), 1–33. <https://doi.org/10.1046/j.1365-2427.1997.00143.x>
- Chang, S., & Wen, C. (1997). Changes in water quality in the newly impounded subtropical feitsui reservoir, Taiwan. *Journal of the American Water Resources Association*, *33*(2), 343–357. <https://doi.org/10.1111/j.1752-1688.1997.tb03514.x>
- Chen, Q., Shi, W., Huisman, J., Maberly, S. C., Zhang, J., Yu, J., et al. (2020). Hydropower reservoirs on the upper Mekong River modify nutrient bioavailability downstream. *National Science Review*, *7*(9), 1449–1457. <https://doi.org/10.1093/nsr/nwaa026>
- Chen, X., Zhang, S., Liu, D., Yu, Z., Zhou, S., Li, R., et al. (2019). Nutrient inputs from the leaf decay of *Cynodon dactylon* (L.) Pers in the water level fluctuation zone of a Three Gorges tributary. *Science of the Total Environment*, *688*, 718–723. <https://doi.org/10.1016/j.scitotenv.2019.06.357>
- Christensen, M., & Frigaard, P. (1994). Design of absorbing wave maker based on digital filters. International Symposium of Wave Physical and Numerical Modeling, Canada.
- Dähnke, K., & Thamdrup, B. (2013). Nitrogen isotope dynamics and fractionation during sedimentary denitrification in Boknis Eck, Baltic Sea. *Biogeochemistry*, *105*(5), 3079–3088. <https://doi.org/10.5194/bg-10-3079-2013>
- Deng, D., Ding, B., He, G., Ji, M., Yang, Y., Liu, G., et al. (2023). The contribution of anammox to nitrogen removal is greater in bulk soils than in rhizosphere soils in riparian wetlands along the Yangtze River. *Global Biogeochemical Cycles*, *37*(5), e2022GB007576. <https://doi.org/10.1029/2022gb007576>
- Fan, C., Zhang, L., Yang, L., Huang, W., & Xu, P. (2002). Simulation of internal loadings of nitrogen and phosphorus in a lake. *Oceanologia et Limnologia Sinica*, *33*, 370–378. (in Chinese).
- Fischer, H., Kloep, F., Wilczek, S., & Pusch, M. T. (2005). A river's liver—microbial processes within the hyporheic zone of a large lowland river. *Biogeochemistry*, *76*(2), 349–371. <https://doi.org/10.1007/s10533-005-6896-y>
- Gao, Q., Li, Y., Cheng, Q., Yu, M., Hu, B., Wang, Z., & Yu, Z. (2016). Analysis and assessment of the nutrients, biochemical indexes and heavy metals in the Three Gorges Reservoir, China, from 2008 to 2013. *Water Research*, *92*, 262–274. <https://doi.org/10.1016/j.watres.2015.12.055>
- Gu, C., Anderson, W., & Maggi, F. (2012). Riparian biogeochemical hot moments induced by stream fluctuations. *Water Resources Research*, *48*(9), W09546. <https://doi.org/10.1029/2011wr011720>
- Guo, J., Jiang, X., Zhou, X., Meng, Y., & Jia, Z. (2016). Impact of periodical flooding-drying on nitrification and ammonia oxidizers in hydro-fluctuation belt of the Three Gorges Reservoir. *Acta Microbiologica Sinica*, *56*(6), 983–999.
- Harrison, J. A., Deemer, B. R., Birchfield, M. K., & O'Malley, M. T. (2017). Reservoir water-level drawdowns accelerate and amplify methane emission. *Environmental Science & Technology*, *51*(3), 1267–1277. <https://doi.org/10.1021/acs.est.6b03185>
- He, D., Wang, K., Pang, Y., He, C., Li, P., Li, Y., et al. (2020). Hydrological management constraints on the chemistry of dissolved organic matter in the Three Gorges Reservoir. *Water Research*, *187*, 116413. <https://doi.org/10.1016/j.watres.2020.116413>
- Hu, N., Liu, D., Ji, D., & Yang, Z. (2012). Effect of backward flow from mainstream on nutrients distribution of tributaries in Three Gorges Reservoir(China). *Environmental Science & Technology*, *35*(10), 6–11.
- Jiang, Q., Jin, G., Tang, H., Xu, J., & Jiang, M. (2022). Ammonium (NH₄⁺) transport processes in the riverbank under varying hydrologic conditions. *Science of the Total Environment*, *826*, 154097. <https://doi.org/10.1016/j.scitotenv.2022.154097>
- Jin, D., Li, J., Gong, J., Li, Y., Zhao, Z., Li, Y., et al. (2021). Shipborne mobile Photogrammetry for 3D Mapping and Landslide detection of the water-level fluctuation zone in the three Gorges reservoir area, China. *Remote Sensing*, *13*(5), 1007. <https://doi.org/10.3390/rs13051007>
- Kang, P., Xu, J., Wang, F., Zhang, H., & Zhao, H. (2024). Characterizing the impact of reservoir storage and discharge on nitrogen dynamics in an upstream wetland using a δ¹⁵N and δ¹⁸O dual-isotope approach. *Science of the Total Environment*, *931*, 172923. (online). <https://doi.org/10.1016/j.scitotenv.2024.172923>
- Keller, P. S., Marcé, R., Obrador, B., & Koschorreck, M. (2021). Global carbon budget of reservoirs is overturned by the quantification of drawdown areas. *Nature Geoscience*, *14*(6), 402–408. <https://doi.org/10.1038/s41561-021-00734-z>
- Li, H., Yang, M., Lei, T., Zhang, M., Bridgewater, P., Lu, C., et al. (2015). Nitrous oxide emission from the littoral zones of the Miyun Reservoir near Beijing, China. *Hydrology Research*, *46*(5), 811–823. <https://doi.org/10.2166/hh.2014.095>
- Li, S., Deng, Y., Shi, F., Hu, M., Pang, B., Wang, Y., et al. (2019). Research progress on water-level-fluctuation zones of reservoirs: A review. *Wetland Science*, *17*(6), 689–696. (in Chinese).
- Li, X., Liu, B., Wang, Y., Yang, Y., Liang, R., Peng, F., et al. (2020). Hydrodynamic and environmental characteristics of a tributary bay influenced by backwater jacking and intrusions from a main reservoir. *Hydrology and Earth System Sciences*, *24*(11), 5057–5076. <https://doi.org/10.5194/hess-24-5057-2020>
- Li, Z., Wang, S., Guo, J., Fang, F., Gao, X., & Long, M. (2012). Responses of phytoplankton diversity to physical disturbance under manual operation in a large reservoir, China. *Hydrobiologia*, *684*(1), 45–56. <https://doi.org/10.1007/s10750-011-0963-2>
- Lin, J., Tang, Y., Liu, D., Zhang, S., Lan, B., He, L., et al. (2019). Characteristics of organic nitrogen fractions in sediments of the water level fluctuation zone in the tributary of the Yangtze River. *Science of the Total Environment*, *653*, 327–333. <https://doi.org/10.1016/j.scitotenv.2018.10.394>
- Liu, D. (2022). Data of flood control reservoirs in China.xlsx. [Dataset]. <https://doi.org/10.6084/m9.figshare.19594009.v1>
- Liu, D. (2023). Main data. [Dataset]. <https://doi.org/10.6084/m9.figshare.26045761.v1>
- Liu, D., Zhao, J., Jeon, W., & Lee, J. (2019). Solute dynamics across the stream-to-riparian continuum under different flood waves. *Hydrological Processes*, *33*(20), 2627–2641. <https://doi.org/10.1002/hyp.13515>
- Liu, L., Liu, D., Johnson, D. M., Yi, Z., & Huang, Y. (2012). Effects of vertical mixing on phytoplankton blooms in Xiangxi bay of three Gorges reservoir: Implications for management. *Water Research*, *46*(7), 2121–2130. <https://doi.org/10.1016/j.watres.2012.01.029>
- Liu, T., Xia, X., Liu, S., Mou, X., & Qiu, Y. (2013). Acceleration of denitrification in turbid rivers due to denitrification occurring on suspended sediment in oxic waters. *Environmental Science & Technology*, *47*(9), 4053–4061. <https://doi.org/10.1021/es304504m>
- Lu, J., Faggoter, S. J., Bunn, S. E., & Burford, M. A. (2017). Macrophyte beds in a subtropical reservoir shifted from a nutrient sink to a source after drying then rewetting. *Freshwater Biology*, *62*(5), 854–867. <https://doi.org/10.1111/fwb.12904>
- Lv, F., Ouyang, W., Song, Y., Cai, C., Hao, R., & Wang, J. (2019). Simulation study on the effects of *Cynodon dactylon* and *Alternanthera philoxeroides* on soil nitrogen and phosphorus release in the reservoir water-level fluctuation zone. *Journal of Soil and Water Conservation*, *33*(3), 240–245. (in Chinese).

- Mahmood, M. N., Schmidt, C., Fleckenstein, J. H., & Trauth, N. (2019). Modeling the impact of stream discharge events on riparian solute dynamics. *Ground Water*, 57(1), 140–152. <https://doi.org/10.1111/gwat.12664>
- Ministry of Environment Protection of the People's Republic of China. (2002). *The monitoring analysis method of water and wastewater*. China Environmental Science Press.
- Mulholland, P. J., Helton, A. M., Poole, G. C., Hall, R. O., Hamilton, S. K., Peterson, B. J., et al. (2008). Stream denitrification across biomes and its response to anthropogenic nitrate loading. *Nature*, 452(7184), 202–205. <https://doi.org/10.1038/nature06686>
- Pan, H., Xu, X., & Gao, S. (2008). Study on process of nutrition release during the decay of submerged macrophytes. *Research of Environmental Sciences*, 21(1), 64–68. (in Chinese).
- Qu, H., & Kroeze, C. (2010). Past and future trends in nutrients export by rivers to the coastal waters of China. *Science of the Total Environment*, 408(9), 2075–2086. <https://doi.org/10.1016/j.scitotenv.2009.12.015>
- Seeley, M. E., Song, B., Passie, R., & Hale, R. C. (2020). Microplastics affect sedimentary microbial communities and nitrogen cycling. *Nature Communications*, 11(1), 2372. <https://doi.org/10.1038/s41467-020-16235-3>
- Shi, W., Chen, Q., Zhang, J., Zheng, F., Liu, D., Yi, Q., & Chen, Y. (2020). Enhanced riparian denitrification in reservoirs following hydropower production. *Journal of Hydrology*, 583, 124305. <https://doi.org/10.1016/j.jhydrol.2019.124305>
- Shi, W., Du, M., Ye, C., & Zhang, Q. (2021). Divergent effects of hydrological alteration and nutrient addition on greenhouse gas emissions in the water level fluctuation zone of the Three Gorges Reservoir, China. *Water Research*, 201(6), 117308. <https://doi.org/10.1016/j.watres.2021.117308>
- Shuai, P., Cardenas, M. B., Knappett, P. S., Bennett, P. C., & Neilson, B. T. (2017). Denitrification in the banks of fluctuating rivers: The effects of river stage amplitude, sediment hydraulic conductivity and dispersivity, and ambient groundwater flow. *Water Resources Research*, 53(9), 7951–7967. <https://doi.org/10.1002/2017wr020610>
- Song, C., Fan, C., Zhu, J., Wang, J., Sheng, Y., Liu, K., et al. (2022). A comprehensive geospatial database of nearly 100,000 reservoirs in China. *Earth System Science Data*, 14(9), 4017–4034. <https://doi.org/10.5194/essd-14-4017-2022>
- Storey, R. G., Williams, D. D., & Fulthorpe, R. R. (2004). Nitrogen processing in the hyporheic zone of a pastoral stream. *Biogeochemistry*, 69(3), 285–313. <https://doi.org/10.1023/b:biog.0000031049.95805.ec>
- Tang, T., Ren, Z., Tang, T., & Cai, Q. (2016). Total nitrogen and total phosphorus thresholds for epilithic diatom assemblages in inflow tributaries of the Three Gorges Reservoir, China. *Chinese Journal of Applied Ecology*, 27(8), 2670–2678.
- Thamdrup, B., & Dalsgaard, T. (2002). Production of N₂ through anaerobic ammonium oxidation coupled to nitrate reduction in marine sediments. *Applied and Environmental Microbiology*, 68(3), 1312–1318. <https://doi.org/10.1128/aem.68.3.1312-1318.2002>
- Trauth, N., Musolff, A., Knöller, K., Kaden, U. S., Keller, T., Werban, U., & Fleckenstein, J. H. (2018). River water infiltration enhances denitrification efficiency in riparian groundwater. *Water Research*, 130, 185–199. <https://doi.org/10.1016/j.watres.2017.11.058>
- Wang, D., Han, G., Hu, M., Wang, Y., Liu, J., Zeng, J., & Li, X. (2022). Biogeochemical processes of dissolved nitrogen in the backwater zone of a tributary in three Gorges reservoir, China: Implications from the hydrologic processes and isotopic Tracing. *ACS Earth and Space Chemistry*, 6(8), 2104–2113. <https://doi.org/10.1021/acsearthspacechem.2c00172>
- Wang, K., Pang, Y., Gao, C., Chen, L., He, D., Li, P., et al. (2021). Hydrological management affected dissolved organic matter chemistry and organic carbon burial in the Three Gorges Reservoir. *Water Research*, 199, 117195. <https://doi.org/10.1016/j.watres.2021.117195>
- Wang, S., Wang, W., Zhao, S., Wang, X., Hefting, M. M., Schwark, L., & Zhu, G. (2019). Anammox and denitrification separately dominate microbial N-loss in water saturated and unsaturated soils horizons of riparian zones. *Water Research*, 162, 139–150. <https://doi.org/10.1016/j.watres.2019.06.052>
- Wang, Z., Xiao, L., Tan, Q., Tian, L., & Zhu, B. (2019). Nitrogen and phosphorus absorption from soil by the dominant herbaceous species in the water-level-fluctuation zone of the Three Gorges Reservoir. *Mountain Research*, 37(2), 151–160. (in Chinese).
- Welch, C., Cook, P. G., Harrington, G. A., & Robinson, N. I. (2013). Propagation of solutes and pressure into aquifers following river stage rise. *Water Resources Research*, 49(9), 5246–5259. <https://doi.org/10.1002/wrcr.20408>
- Worsfold, P. J., Monbet, P., Tappin, A. D., Fitzsimons, M. F., Stiles, D. A., & McKelvie, I. D. (2008). Characterisation and quantification of organic phosphorus and organic nitrogen components in aquatic systems: A review. *Analytica Chimica Acta*, 624(1), 37–58. <https://doi.org/10.1016/j.aca.2008.06.016>
- Xia, X., Jia, Z., Liu, T., Zhang, S., & Zhang, L. (2016). Coupled nitrification-denitrification caused by suspended sediment (SPS) in rivers: Importance of SPS size and composition. *Environmental Science & Technology*, 51(1), 212–221. <https://doi.org/10.1021/acs.est.6b03886>
- Xiang, R., Wang, L., Li, H., Tian, Z., & Zheng, B. (2021a). Water quality variation in tributaries of the three Gorges reservoir from 2000 to 2015. *Water Research*, 195, 116993. <https://doi.org/10.1016/j.watres.2021.116993>
- Xiang, R., Wang, L., Li, H., Tian, Z., & Zheng, B. (2021b). Temporal and spatial variation in water quality in the Three Gorges Reservoir from 1998 to 2018. *Science of the Total Environment*, 768, 144866. <https://doi.org/10.1016/j.scitotenv.2020.144866>
- Xiao, L., Zhu, B., Kumwimba, M. N., & Jiang, S. (2017). Plant soaking decomposition as well as nitrogen and phosphorous release in the water-level fluctuation zone of the Three Gorges Reservoir. *Science of the Total Environment*, 592, 527–534. <https://doi.org/10.1016/j.scitotenv.2017.03.104>
- Xu, D., Hai, R., Zheng, B., Qin, Y., & Zhang, L. (2010). Release kinetics of ammonia nitrogen from soils of water-level fluctuating zone in input river of Three Georges Reservoir (China). *Environmental Science & Technology*, 33(10), 49–52.
- Xu, H., Zhang, L., Shang, J., Dai, J., & Fan, C. (2009). Denitrification and anammox on the sediment-water interface in the Meiliang bay of lake Taihu. *Journal of Lake Sciences*, 21(6), 775L781. (in Chinese).
- Yao, X., Zhang, L., Zhang, Y., Xu, H., & Jiang, X. (2016). Denitrification occurring on suspended sediment in a large, shallow, subtropical lake (Poyang Lake, China). *Environmental Pollution*, 219, 501–511. <https://doi.org/10.1016/j.envpol.2016.05.073>
- Ye, C., Cheng, X., Zhang, K., Du, M., & Zhang, Q. (2017). Hydrologic pulsing affects denitrification rates and denitrifier communities in a revegetated riparian ecotone. *Soil Biology and Biochemistry*, 115, 137–147. <https://doi.org/10.1016/j.soilbio.2017.08.018>
- Yu, J., Zhang, Y., Zhong, J., Ding, H., Zheng, X., Wang, Z., et al. (2020). Water-level alterations modified nitrogen cycling across sediment-water interface in the Three Gorges Reservoir. *Environmental Science and Pollution Research*, 27(21), 25886–25898. <https://doi.org/10.1007/s11356-019-06656-z>
- Zhang, A., & Gu, V. (2023). Global dam tracker: A database of more than 35,000 dams with location, catchment, and attribute information. *Scientific Data*, 10(1), 111. <https://doi.org/10.1038/s41597-023-02008-2>
- Zhao, S., Zhang, B., Sun, X., & Yang, L. (2020). Hot spots and hot moments of nitrogen removal from hyporheic and riparian zones: A review. *Science of the Total Environment*, 762, 144168. <https://doi.org/10.1016/j.scitotenv.2020.144168>
- Zhou, N., Zhao, S., & Shen, X. (2014). Nitrogen cycle in the hyporheic zone of natural wetlands. *Chinese Science Bulletin*, 59(24), 2945–2956. <https://doi.org/10.1007/s11434-014-0224-7>